Assessing Various Scenarios of Multitemporal Sentinel-2 Imagery, Topographic Data, Texture Features, and Machine Learning Algorithms for Tree Species Identification

Iosif Vorovencii

***Abstract*—Accurate information about forests, including the identification of tree species, can be achieved by utilizing combinations of various datasets, analyzed over different temporal scales, and employing advanced classification algorithms. Free Sentinel-2 (S-2) satellite imagery, along with other auxiliary data, can serve as valuable sources of geospatial data. In the present study, several scenarios and time intervals were evaluated for tree species identification. Within each scenario, the data were classified using supervised machine learning algorithms random forest (RF) and gradient tree boosting (GTB). The data combinations targeted four scenarios: S-2 bands (scenario 1); S-2 bands and topographic data (scenario 2); S-2 bands and texture features (scenario 3); S-2 bands, topographic data, and texture features (scenario 4). Each scenario was applied for spring, summer, autumn, and long-term intervals. The identified tree species included spruce, beech, fir, larch, pine, mixed species, and other broadleaf species. The best results in tree species identification were obtained in scenario 4. The findings showed that GTB outperformed RF algorithm, providing overall accuracies (OAs) between 96.40% (long-term, scenario 4) and 95.73% (spring, scenario 4). RF was placed second, reaching OAs ranging from 87.41% (long-term, scenario 4) to 84.02% (summer, scenario 4). The integration of topographic data in combinations led to the largest increase in OAs, reaching up to 24.05% percentage point (GTB, summer, scenario 2) in tree species identification. The contribution of texture features in tree species identification was marginal.**

***Index Terms*—Machine learning (ML), scenario, Sentinel-2 (S-2) image, tree species identification.**

I. Introduction

THE ecological benefits provided by forests, such as regulating surface temperature, maintaining hydrological regimes, adjusting local and regional climates, and reducing carbon emissions, are widely acknowledged. Tree species are the most important components of forests, and obtaining information about them is necessary for forest management planning [1]. Secure identification of tree species and their distribution help in monitoring forest biodiversity, assessing ecological changes, understanding forest conditions, and in many other forestry applications [2].

Ground-based identification of forest resources is costly, time-consuming, challenging, and requires highly skilled personnel. Furthermore, this traditional method does not provide detailed information regarding the spatial distribution of tree species, which is necessary for modern forestry resource management [3], and does not allow for a higher update frequency. Remote sensing is the main method for collecting geospatial data used in tree species identification, especially when studies are conducted over large areas. In addition, Google Earth Engine (GEE), which is the world's most advanced cloud platform for processing remote sensing Big Data, provides a rich library of free satellite imagery and facilitates access to dense time series. These images can be used to conduct studies based on seasonal and phenological variations of tree species [4].

Sentinel-2 (S-2) imagery has high potential in various mapping applications, including forest-type classification [5], and tree species identification [6], [7], [8]. The relatively high repetitive cycle of S-2A/B satellites (five days) and higher spatial resolution (10–20 m), allowing for the capture of more detailed information, make these images valuable geospatial data sources. Moreover, the spectral information included in the 13 bands of the S-2 multispectral instrument, especially the red-edge and SWIR bands, shows promise in detecting differences between vegetation features [9], [10]. Studies employing multitemporal S-2 imagery have shown their high potential for mapping forest stand species [6], [8], [11], [12], [13], [14], [15], [16], [17], [18].

In large areas with complex forest composition and environmental conditions, new challenges arise in tree species classification. Different growth conditions, ages of tree species [19], and forest structures lead to a high variability of spectral signatures recorded by the optical bands of S-2 imagery. Therefore, combining S-2 imagery with various auxiliary data can significantly increase the overall accuracy (OA) in tree species identification. Such data can be obtained from gray level co-occurrence matrix (GLCM) and digital elevation model (DEM). By combining spectral data with texture features, such as texture, contrast, entropy, variability, etc., OA can increase by up to 10%–15% [6], [20]. Moreover, topographic data such as elevation, aspect,

Manuscript received 22 March 2024; revised 8 June 2024; accepted 25 July 2024. Date of publication 5 August 2024; date of current version 5 September 2024. This work was supported by Anelis Plus Consortium based on an agreement between Anelis Plus Consortium and Institute of Electrical and Electronics Engineers (IEEE).

The author is with the Transilvania University of Brașov, 500036 Brașov, Romania (e-mail: iosif.vorovencii@unitbv.ro).

Digital Object Identifier 10.1109/JSTARS.2024.3436624

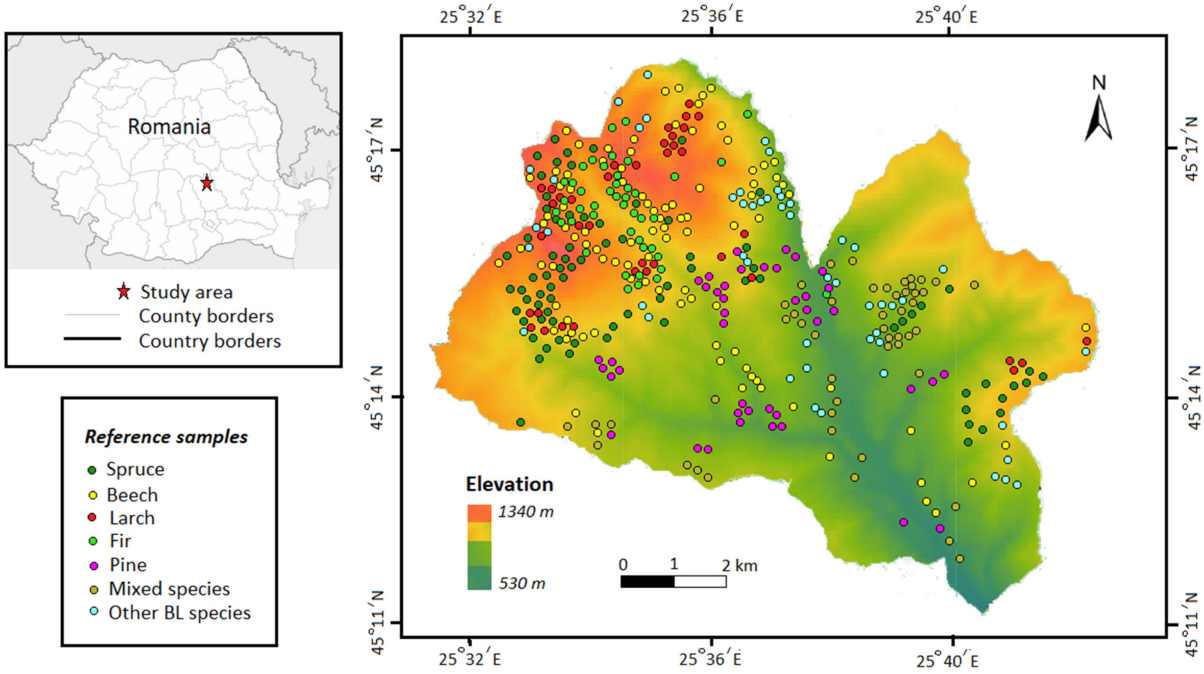

Fig. 1. Research area, represented on the digital terrain model, with the distribution of reference samples. The dots represent the plot center.

and slope obtained from DEM can provide valuable information for tree species discrimination, especially in mountain areas [4]. Since these data influence the altitudinal distribution of tree species, this leads to an increase in OA for the resulting cartographic products.

Processing large and complex datasets composed of multitemporal imagery, topographic data, and textural features is done using machine learning (ML) algorithms [14]. These algorithms are often used for tree species identification and are capable of modeling complex class signatures [21]. ML algorithms have proven to be efficient in classifying high-dimensional data, allowing for the use of a wide variety of data and do not require a statistical distribution of them [21], [22], [23]. In GEE, many ML algorithms are built that can be used in tree species identification, such as random forest (RF) and gradient tree boost (GTB). Several studies have found that these algorithms produce higher accuracy compared to traditional parametric algorithms, especially for complex data, with a high-dimensional feature space [21], [24]. Using ML algorithms requires tuning the parameters to find the optimal input values for obtaining the best OAs. A common problem for most ML algorithms is the risk of overfitting. To reduce this risk, techniques for reducing the number of variables can be applied, thus avoiding model overfitting and contributing to accuracy improvement [23].

The main objective of this study was to assess various scenarios of multitemporal S-2 imagery, topographic data, texture features, and ML algorithms for tree species identification in an area with complex landscape. The specific objectives were as follows:

1) to compare RF and GTB ML algorithms in classifying the datasets used for the defined scenarios and time intervals;
2) to evaluate the defined scenarios for each time interval and ML algorithm;
3) to compare between time-scale intervals;
4) to evaluate tree species identification. The defined scenarios considered different combinations of data, while the time intervals took into account seasonal intervals with significant phenological activity.

II. Materials

A. Study Area

The study was conducted in an area located between 45°10′ – 45°19′ N and 25°31′ – 25°42′ E, situated in the central part of Romania, south of the Bucegi Mountains (see Fig. 1). The terrain is characterized by high hills and the beginning of a mountainous area, where approximately 77% of the slopes have a steep gradient (up to 30°) and 18% have a very steep gradient (over 30°). The study area covers an area of 8519 ha, situated on terrain with an elevation difference of 810 m (530–1340 m above sea level). The average annual temperature is +6.8 °C, and the average annual precipitation is approximately 770 mm.

The predominant tree species (89%) are common beech (*Fagus sylvatica*), Norway spruce (*Picea abies*), silver fir (*Abies alba*), European larch (*Larix decidua*), Scots pine (*Pinus sylvestris*), and black pine (*Pinus nigra*). In smaller proportion, other species include sycamore maple (*Acer pseudoplatanus*), oak (*Quercus petraea ssp. petraea*), gray alder (*Alnus incana*), black alder (*Alnus glutinosa*), European hornbeam (*Carpinus betulus*), aspen (*Populus tremula*), silver birch (*Betula pendula*), European ash (*Fraxinus excelsior*), and willow (*Salix caprea*). Forest management is carried out by the National Forestry Administration (34.5%) and private forestry districts

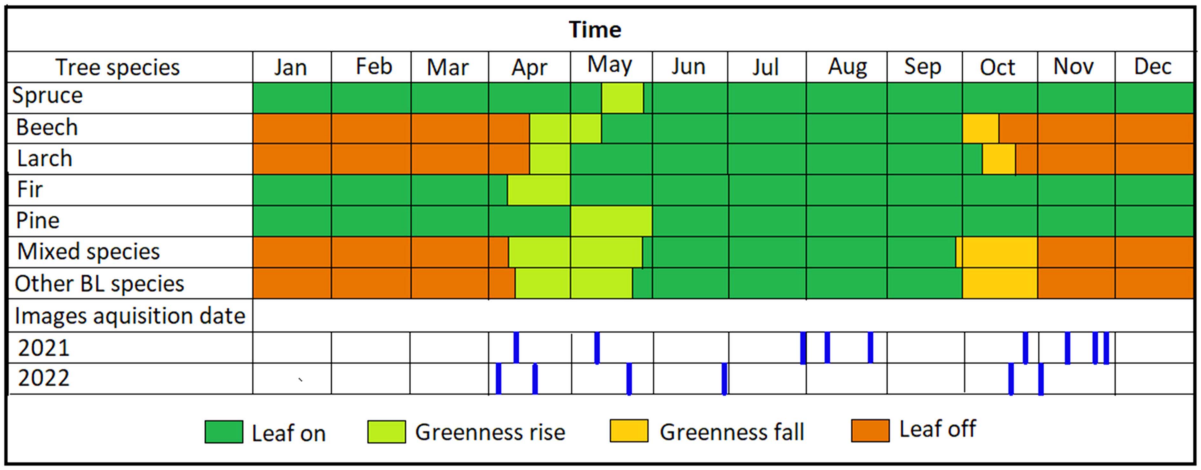

Fig. 2. Tree species phenology and corresponding image acquisition dates, illustrating the relationship between tree phenological phases and image acquisition timing.

(43.3%). The remaining analyzed area (22.2%) consists of pasture, hayfields, and built-up areas (roads, buildings, parking lots, etc.).

The forests in the study area are both pure and mixed stands. In a mixed stand, five–six tree species can be found, with some (two or three) being dominant species and the rest being secondary species. The share of tree species in a stand is specified in the forest management plan and was determined through forest inventory. Species with less representation in the stand (below 10%) appear in the forest management plan as other species.

B. Satelite Imageries

In total, 15 scenes of S-2 imagery were used, acquired in the years 2021 and 2022, from April 1st to November 26th (see Fig. 2). The images belong to relative orbit number 50, tile number T35TLL, and were freely downloaded from the Copernicus Data Hub. These images are orthorectified and atmospherically and topographically corrected at Level-2A (Bottom of Atmosphere). The spectral bands of the S-2 images used in the study were: B2, B3, B4, B5, B6, B7, B8, B8a, B11, and B12. In addition, coastal aerosol, water vapor, and cirrus bands were excluded from further processing. The images are in the WGS 84 projection, zone 35N.

C. DEM and Extraction of Texture Features

The DEM with a spatial resolution of 30 m was downloaded from the archive available in the GEE platform. It was clipped to the outline of the study area and resampled to a 20 m resolution using the bilinear resampling method. Processing the DEM resulted in slope and aspect, which, along with elevation, constituted the topographic data used as auxiliary data in different combinations with S-2 images and texture features. In GEE, scaling is performed automatically, ensuring that all bands used in various combinations are correctly overlaid.

The GLCM is used in remote sensing to extract texture features. GLCM calculates the gray levels of pixels in the image and provides a series of statistical indicators. Haralick et al. [25] proposed 14 statistics, while Conners et al. [26] proposed an additional four statistics that can be calculated based on GLCM. The feature selection procedure involves choosing a subset or a linear combination of features available through two methods: 1) using a set of training image regions to establish a set of features that result in the smallest classification errors; 2) using some functional feature space distance metric such that a large feature space distance implies a small classification error [27]. Gotlieb and Kreyszig [28] found that groups of four features were optimal.

To calculate GLCM, S-2 images were rescaled to a 16-bit integer range. For spatial texture estimation, the near-infrared band (B8) from S-2 composite images (2021 and 2022) was used, based on a 4-pixel-wide with 3×3 square kernel. We chose the near-infrared band because it contains spectral information suitable for differentiating vegetation characteristics. In total, five texture features were calculated by processing GLCM in GEE: entropy (EN), variance (VAR), correlation (COR), contrast (CO), and homogeneity (HO) (see Table I). The entropy value indicates the complexity of the image in terms of the distribution of gray values; for complex images, entropy values are larger, and vice versa. Variance is a measure of the distribution of gray values in the analyzed image. The correlation shows the level of similarity of gray values along the rows or columns. Contrast represents the texture characteristics and image clarity; high values reflect significant correlation. Homogeneity is calculated within a processing window and expresses the similarity measure of pixel values. Texture features, as well as topographic data in different combinations with spectral bands of S-2 images, served as input data for each ML algorithm.

D. Reference Data

The official forestry database of the state forest administration from the National Institute for Research and Development in

TABLE I
TEXTURE FEATURES FORMULAS USED IN THIS STUDY

Texture features			Formulas	Applications
Type	Acronym	Acronym used in GEE		
Entropy	EN	B8_ent	$-\sum_{i}^{N}\sum_{j}^{N} P(i,j\|d,\theta) log_2 P(i,j\|d,\theta)$	Evaluating the entropy of the GLCM [29] Depicting the complexity of the texture's distribution [30]
Variance	VAR	B8_var	$\sum_{i}^{N_g}\sum_{j}^{N_g}(i-\mu)^2 p(i,j)$	Tree species classification based on S-2 imagery [2].
Correlation	COR	B8_corr	$\frac{\sum_i^N \sum_j^N (i-\bar{x})(j-\bar{y})P(i,j\|d,\theta)}{\sigma_x \sigma_y}$	Assessing the linear correlation of gray levels across pixels [29], [30]. Tree species classification in mixed deciduous forests using very high spatial resolution satellite imagery [31].
Contrast	CON	B8_contrast	$-\sum_{i}^{N}\sum_{j}^{N}\|i-j\|^2 p(i,j)$	Tree species classification based on S-2 imagery [2]. Tree species classification in mixed deciduous forests using very high spatial resolution satellite imagery [31].
Homogeneity	HO	B8_idm	$-\sum_{i}^{N}\sum_{j}^{N}\frac{P(i,j\|d,\theta)}{1+(i-j)^2}$	Quantifying the level of uniformity within a pair of pixels [29]. Vegetation mapping using S-2 [16].

Forestry "Marin Drăcea" from Romania constituted the reference data. It included data from Forest Management Unit (FMU) I Comarnic and FMU II Posada, both within the Sinaia Forestry District. In FMU I Comarnic, state-managed forests cover an area of 2091.6 ha, supplemented by 907.7 ha of private forests. FMU II Posada has an area of 850.9 ha covered by state forests, to which private forests are also added. The field boundaries of the two FMUs consist of natural features (water bodies, ridges, valleys) or artificial features (roads, railways, etc.) represented by characteristic symbols. Within the two FMUs, in the urban areas of the localities, there are parcels of forests of various sizes, compositions, and structures.

The forestry database includes graphical data and attributes of each forest unit, which constitutes the minimum recorded unit. The graphical data comprise polygons delineating each forest unit and are defined by coordinates on the outline expressed in the Stereographic 1970 projection, which is the official projection of Romania. In the present study, the boundaries of FMUs and forest units were converted from Stereographic 1970 to WGS 84 projection, Zone 35 N [32], [33]. The boundaries of the two FMUs, along with forest units, were merged in QGIS and imported into the GEE *via* Google Fusion Tables. The attributes from the forestry database include data related to species composition, attributes of stands (stand structure, stand density, age, height, medium diameter, volume, etc.), site characteristics (soil, geology, slope, orientation, etc.), and many other types of information.

A forest unit represents the minimum recorded unit in the forest management plan. The establishment of forest units was based on silvicultural criteria used in forest inventory to delimit homogeneous stands. These criteria include:

1) encompassing a single ecosystem or site unit;

2) having the same density or a density difference not exceeding 0.2 (on a scale from 0 to 1);

3) having the same composition, with differences not exceeding 20% for the main species (on a scale from 0 to 100);

4) the average age not differing by more than 20 years;

5) presenting a similar structure type (even-aged, relatively even-aged, relatively uneven-aged, uneven-aged);

6) having a single productivity category.

FMU I Comarnic comprises 355 forest units, while FMU II Posada has 111 forest units. Approximately 60 forest units located mainly in the southern part of the study area were also analyzed in private forests. In the forestry database, each forest unit is demarcated by a polyline that has known coordinates; in the field, demarcation is done using paint signs on trees [34], [35]. The forest units ranged in size from 0.2 to 44.3 ha (average 5.9 ha) for FMU I Comarnic and from 0.1 to 31.8 ha (average 7.7 ha) for FMU II Posada.

Forest management plans are updated every ten years. Major changes occurring during these ten years, such as cuttings and windthrows, are recorded annually [36]. In this way, the forestry database is continuously updated and includes all changes affecting each stand at the time they occur. Part of the data from the forestry database was validated through field trips in 2022. As secondary products used for validation, orthophotoplans from the National Agency for Cadastre and Land Registration and Google Earth images were also employed.

TABLE II
NUMBER AND AREA OF TRAINING AND VALIDATION POLYGONS FOR ALL TREE SPECIES

Tree species	Training polygons		Validation polygons	
	No. polygons	Area (ha)	No. polygons	Area (ha)
Spruce	63	57.7	16	14.2
Beech	75	97.2	19	24.1
Larch	30	10.7	8	2.4
Fir	36	16.6	9	3.9
Pine	34	14.6	8	3.4
Mixed species	38	8.8	10	2.0
Other BL species	41	18.5	10	4.3
Total	317	224.1	80	54.3

E. Training and Validation Data

Samples for training and validation were collected from pure stands listed in the official forestry database and were previously confirmed during a field trip. The collection of spectral signatures was performed within polygons located in the middle of the forests, thus avoiding marginal areas that may interfere with species from neighboring stands. The number and area occupied by the polygons created for each tree species or group of species are presented in Table II.

The reference samples were randomly divided, with 80% used for training and 20% for accuracy assessment. The separation into training and validation was made at the stock level. In this sense, each sample was assigned a stock that had an associated attribute used to differentiate the stocks within the analysis. All defined stocks were added to a collection and were randomly split into training and validation sets by adding a random column to each stock. The splitting method ensures that all points in the same stock are treated together, so the separation is consistent at the stock level. In the case of generating the forest/nonforest map, the total number of pixels was 14 525, with 11 621 pixels for training and 2904 pixels for validation. For tree species identification, a total of 6961 pixels were used, with 5603 for training and 1358 pixels for validation.

An accuracy assessment was conducted based on the confusion matrix. For each classified map, OA, producer's accuracy (PA), user's accuracy (UA), and F1-score were calculated. In addition, quantity disagreement and allocation disagreement were determined instead of the Kappa coefficient. Quantity disagreement evaluates the absolute disparities in proportions between the reference map and a comparison map across different categories [37]. This metric arises when there are varying numbers of pixels for each category in the two maps, and it is calculated using the following equations [37]:

$$q_g = \left| \left(\sum_{i=1}^{J} p_{ig} \right) - \left(\sum_{j=1}^{J} p_{gi} \right) \right| \tag{1}$$

$$Q = \frac{\sum_{g=1}^{J} q_g}{2} \tag{2}$$

where q_g represents the quantity disagreement for a specific category g, while p_{ig} and p_{gi} indicate the estimated proportion of that category in both the simulation and reference maps, respectively; Q stands for the overall quantity.

Allocation disagreement indicates the difference between observed and simulated maps, stemming from inconsistencies in the spatial distribution of categories, and is computed using the following equation [37]:

$$a_g = 2 \min \left[\left(\sum_{i=1}^{J} p_{ig} \right) - p_{gg}, \left(\sum_{j=1}^{J} p_{gi} \right) - p_{gg} \right] \tag{3}$$

$$A = \frac{\sum_{g=1}^{J} a_g}{2} \tag{4}$$

where a_g represents the allocation disagreement for a specific category g, p_{gg} denotes the proportion of category g from the observed data that is allocated to category g in the simulated map, and A represents overall allocation. The overall disagreement (D) is the aggregate of quantity disagreement and allocation disagreement [37].

After applying ML algorithms, the importance of variables was estimated in GEE by computing the normalized and raw variable importance. In addition, McNemar's test was employed to highlight statistically significant relationships between ML algorithms.

III. METHODS

A. Machine Learning Algorithms and Tuning Parameters

In this study, we employed the RF and GTB ML algorithms available in the GEE platform. For each classifier, a series of values were used and tested in the tuning process to find the optimal parameters ensuring the highest OA for classification. The flowchart of the research is illustrated in Fig. 3.

RF is a fast, easily parameterizable, robust algorithm [38] commonly used for land use and land cover classification [39], [40] as well as for tree species classification [41], [42], [43]. The RF classifier consists of Ntree, where N is the number of trees to be grown, defined by the user. When classifying a new dataset, it passes through each of these N trees. The RF classifier selects the class with the most votes from N, for that particular case. The parameters for which the optimal value needed to be found are the number of trees (Ntree) and the variables used in each node (mTry). Studies have shown that to achieve satisfactory and stable results, Ntree should be between 200 and 500 [44]. In this study, to find the optimal parameters of the RF model, Ntree values were tested in the range of 50–600, with a step size of 50; for mTry, the tested values were in the range of 1–15, with a step size of 1.

GTB, similar to RF, employs an ensemble of decision trees but, unlike RF, it restricts the complexity of the trees. To reduce the correlation between trees, each new tree is created based on the randomized selection of subsamples from the complete training data [45]. These subsamples are then used to fit the base learner and update the model for the next iteration, gradually reducing the cumulative model loss [46]. Studies have shown

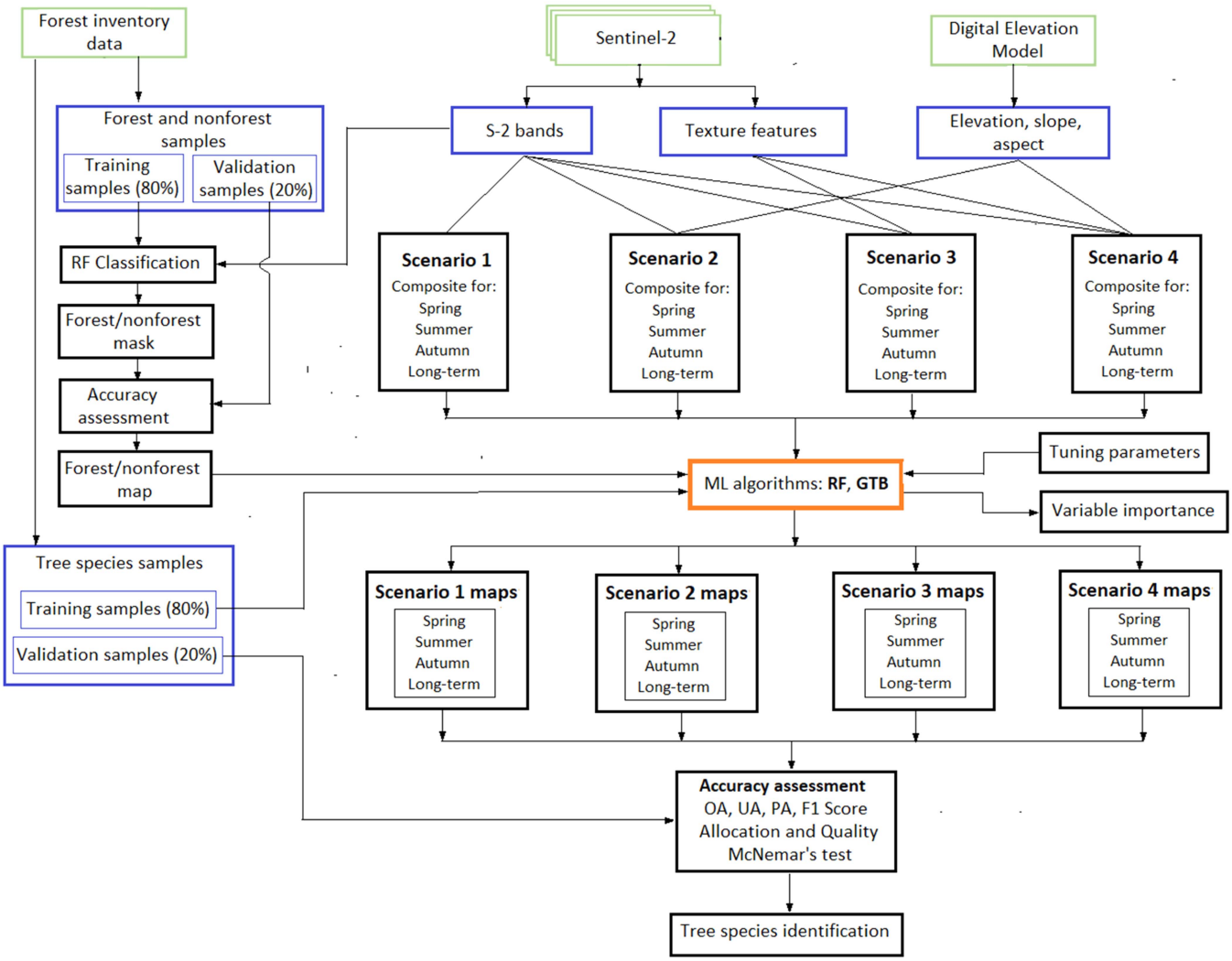

Fig. 3. Flowchart illustrating the step-by-step process of the research methodology and analysis. Before making the composite, the temporal intervals (spring, summer, autumn, and long-term) were defined.

that GTB algorithms, such as Xgboost, outperform RF, support vector machine, and K-nearest neighbor algorithms [47], mainly on unbalanced datasets. However, GTB algorithms are prone to overfitting, but this risk can be minimized through parameter tuning [45].

The GTB algorithm parameters tuned in this study are the number of trees (Ntree), maxNodes, sampling rate, shrinkage rate, and loss. Regarding Ntree, the tested values were between 50 and 200, with a step size of 10. Although the literature generally recommends Ntree to be 1000 [48], the maximum value tested in this study was 200. The maxNodes parameter was in the range of 2–10, with a step size of 1. The two parameters that control the learning rate of the algorithm, namely the sampling rate and shrinkage rate, were also optimized. For the sampling rate, values in the range of 0.40–0.80 were tested, with a step size of 0.05. In the case of the shrinkage rate, the tested values were 0.01, 0.05, 0.1, 0.25, and 0.5. In addition, the three loss functions available in GEE for GTB, namely least squares, least absolute deviation, and Huber, were compared.

B. *Forest Tree Species Identification*

The identification of tree species was carried out in two stages. In the first stage, a forest mask was built using all S-2 images and the RF classifier, which is easier to parameterize, to retain only forested areas. For training and validation, 193 samples were used, consisting of 84 samples for forest and 109 for nonforest. These were visually selected and delineated through polygons. The nonforest class consists of built-up areas (roads, buildings, etc.), agricultural lands (hay, pasture, arable), and water. In the second stage, tree species were identified within the forest mask using the three ML algorithms.

We defined four different time scales, including spring, summer, autumn, and long-term intervals of time (see Table III). Within each temporal interval, various classification datasets (scenarios) were defined, with different combinations of input variables. Thus, in the study, for each scenario, a composite was created that included the S-2 bands from the analyzed time interval. The composites were created using the median of the bands, resulting in multitemporal composites for each band. In

TABLE III
TEMPORAL INTERVALS USED FOR CALCULATING SEASONAL AND LONG-TERM COMPOSITES BETWEEN 2021 AND 2022

Time scales	Acronym	Intervals between 2021 and 2022
Seasonal	spr	April 1 to May 31 (spring - start of the growing season)
	sum	June 1 to August 31 (summer - peak of the growing season)
	aut	September 1 to November 26 (autumn - end of the growing season)
Long-term	lg	April 1 to November 26

TABLE IV
SCENARIOS NAME, NUMBER, AND NAME OF SELECTED VARIABLE USED IN THE STUDY FOR EVERY TEMPORAL INTERVAL

Scenario		Name of selected variables
Name	Number of variables in each scenario	
1_spr	50	B2, B3, B4, B5, B6, B7, B8, B8A, B11, B12
1_sum	40	
1_aut	60	
1_lg	150	
2_spr	53	B2, B3, B4, B5, B6, B7, B8, B8A, B11, B12, elevation, slope, aspect
2_sum	43	
2_aut	63	
2_lg	153	
3_spr	55	B2, B3, B4, B5, B6, B7, B8, B8A, B11, B12, EN, VAR, COR, CON, HO
3_sum	45	
3_aut	65	
3_lg	155	
4_spr	58	B2, B3, B4, B5, B6, B7, B8, B8A, B11, B12, elevation, slope, aspect, EN, VAR, COR, CON, HO
4_sum	48	
4_aut	68	
4_lg	158	

Notes:
1_spr – scenario 1 spring, 1_sum – scenario 1 summer, 1_aut – scenario 1 autumn, 1_lg – scenario 1 long-term
2_spr – scenario 2 spring, 2_sum – scenario 2 summer, 2_aut – scenario 2 autumn, 2_lg – scenario 2 long-term
3_spr – scenario 3 spring, 3_sum – scenario 3 summer, 3_aut – scenario 3 autumn, 3_lg – scenario 3 long-term
4_spr – scenario 4 spring, 4_sum – scenario 4 summer, 4_aut – scenario 4 autumn, 4_lg – scenario 4 long-term
B2, B3, B4, B5, B6, B7, B8, B8A, B11, B12 – represent the optical bands of S-2 used in study
EN—entropy, VAR— variance, COR—correlation, CO—contrast, HO—homogeneity

the case of scenarios 2, 3, and 4, the other variables were added to these composites. Thus, for each temporal interval, 4 scenarios were established, totaling 16 scenarios (see Table IV).

The dominant tree species in the area were spruce, beech, larch, fir, and pine. A separate class was formed for each tree species. In addition to these, two groups of tree species were identified, each forming separate classes. In the first group, called other broadleaves species (other BL species), broadleaves tree species found in the forest management plan with a share of less than 10% were included. In the second group, called mixed species class, tree species located at lower altitudes, primarily found in urban areas, were included. The species in this class are both coniferous and broadleaves, found in patches of various sizes and shapes, and could not be assigned to classes with dominant species due to their intimate grouping pattern.

IV. RESULTS

A. Optimal Tuning Parameters

Most ML algorithms require hyperparameter tuning. Optimizing hyperparameters is a key aspect of the ML algorithm training process, and optimal parameter values vary across sites; therefore, an extensive grid search is needed [49]. The tuned parameters based on which the highest OAs were obtained for each scenario, classifier, and time-scale interval are presented in Table V. For GTB, the Ntree ranged from 160 to 190, with maxNodes set to no limit. The shrinkage function showed optimal values between 0.05 and 0.50, with the most frequent value being 0.10, while for the sampling rate, the values ranged from 0.40 to 0.80. The type of loss function used had a negligible effect on OAs, as highlighted in other studies [45]. For RF, the Ntree used for the final analysis varied between 50 and 600, and mTry was between 1 and 12. The greater variation in Ntree for RF may be due to the complexity and variability of the data, meaning that datasets with higher variability required a larger number of trees to ensure model accuracy. In addition, it is possible that the dimensions of the training data samples influence the optimal number of trees. Thus, larger datasets may require a greater number of trees to cover the data variability.

Table VI lists the results obtained after applying McNemar's test. The results show that in scenarios 2 and 4, there is a significant difference between RF and GTB regarding the test

TABLE V
VALUES OF TUNING PARAMETERS FOR OPTIMAL ACCURACIES FOR EACH SCENARIO, CLASSIFIER, AND TIME-SCALE INTERVAL

Scenario	Classifier	Parameter	Time scales			
			Spring	Summer	Autumn	Long-term
(1) Spectral features	RF	Ntree	400	100	500	250
		mTry	4	5	8	1
	GTB	Ntree	190	180	190	190
		maxNodes			no limit	
		shrinkage	0.10	0.10	0.25	0.10
		samplingRate	0.50	0.70	0.80	0.40
		loss function	-	-	-	-
(2) Spectral features + topographic features	RF	Ntree	400	450	200	500
		mTry	3	12	5	8
	GTB	Ntree	190	190	170	190
		maxNodes			no limit	
		shrinkage	0.50	0.10	0.10	0.25
		samplingRate	0.80	0.80	0.70	0.70
		loss function	-	-	-	-
(3) Spectral features + texture features	RF	Ntree	500	50	400	600
		mTry	11	3	6	12
	GTB	Ntree	170	160	190	180
		maxNodes			no limit	
		shrinkage	0.10	0.10	0.10	0.05
		samplingRate	0.70	0.70	0.80	0.70
		loss function	-	-	-	-
(4) Spectral features + topographic features + texture feature	RF	Ntree	400	250	550	300
		mTry	8	4	6	1
	GTB	Ntree	190	190	180	190
		maxNodes			no limit	
		shrinkage	0.10	0.10	0.10	0.25
		samplingRate	0.80	0.80	0.80	0.80
		loss function	-	-	-	-

TABLE VI
RESULTS OF APPLYING THE MCNEMAR'S TEST

Scenario	Time-scale interval	Comparison	χ^2	p-value
Scenario 1	Spring	RF versus GTB	0.92	0.34
Scenario 2			18.9	<0.0001
Scenario 3			7.31	0.007
Scenario 4			71.33	<0.0001
Scenario 1	Summer	RF versus GTB	0.21	0.32
Scenario 2			74.97	<0.0001
Scenario 3			11.68	<0.001
Scenario 4			76.95	<0.0001
Scenario 1	Autumn	RF versus GTB	0.84	0.36
Scenario 2			59.86	<0.0001
Scenario 3			16.31	<0.0001
Scenario 4			75.31	<0.0001
Scenario 1	Long-term	RF versus GTB	2.36	0.12
Scenario 2			48.93	<0.0001
Scenario 3			11.49	<0.001
Scenario 4			67.35	<0.0001

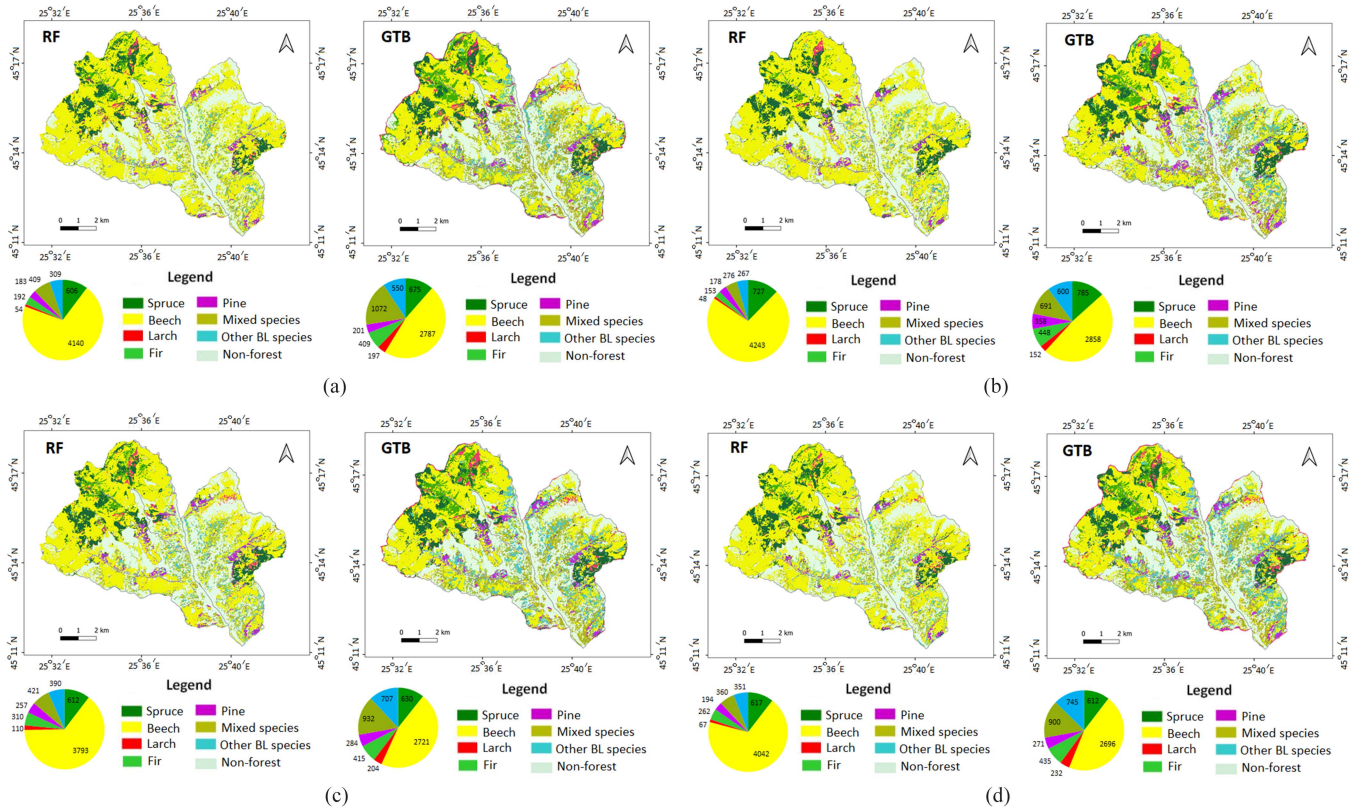

Fig. 4. Maps depicting the distribution of tree species identified in the studied area using RF and GTB ML algorithms (scenario 4). The pie chart illustrates the areas (in hectares) occupied by tree species. (a) Spring. (b) Summer. (c) Autumn. (d) Long-term.

outcomes, and this difference cannot be attributed to chance. This indicates that, in this specific context, one of the ML algorithms, primarily GTB, has yielded more accurate results than RF.

B. Overall Accuracy Assessment

After applying the three ML algorithms to each scenario and time interval, maps illustrating the distribution of each tree species were generated (see Fig. 4). Fig. 5 displays a map representing the best result achieved, specifically for the long-term interval in scenario 4 using GTB.

The achieved OAs depend on the ML algorithm, the type of datasets, and the time-scale intervals. These range between 70.54% and 96.40% and are presented in Fig. 6. GTB has led to the highest OAs for scenario 4, exceeding 95%, in all time intervals, which implies the combination of S-2 spectral bands, topographic data, and textural features. The OAs values for GTB are very close in scenario 4, with a difference of 0.67%pt. (percentage point) between the highest (96.40%, long-term) and the lowest (95.73%, spring). RF also yields high values (over 84%) in scenario 4 using the same combination of S-2 spectral bands, topographic data, and texture features.

Regarding the datasets used, the OAs have significantly increased for all ML algorithms and time scales in scenario 2 by adding topographic data to spectral features (see Fig. 6). For example, for the summer interval, the OA increased by 24.05%pt. for GTB and by 13.58%pt. for RF. It is possible that in this case, the significant increase in OA is due to topographic data rather than phenological processes, which are less visible in summer satellite images; also, the number of summer bands used to create the composite was lower. The smallest increase in OA was 9.38%pt. and was encountered in RF in autumn for scenario 2. Relative to spectral features (scenario 1), the addition of texture features (scenario 3) led to a moderate increase in OA ranging from 1.69%pt. (RF, autumn) to 8.64%pt. (GTB, summer). In the long-term interval, by adding texture features, OA even decreased by 1.12%pt. for RF (see Figs. 6 and 7).

Related to OAs obtained from temporal intervals, the highest values were obtained in the long-term and autumn. Thus, in the long-term interval, GTB led to the highest OA for scenario 4 (96.40%), and in autumn for scenarios 1–3 (78.16%, 95.39%, and 84.64%, respectively). In contrast, RF resulted in high OAs in the long-term interval (scenarios 1, 2, and 4–76.50%, 86.60%, and 87.41%) and in the autumn interval (scenario 3–77.81%).

The highest overall disagreements were estimated for RF for all intervals, with the highest values in autumn (12.72%) and spring (9.72%) (see Fig. 8). The lowest overall disagreement values were obtained by GTB in all cases, with 4.66% for the long-term interval and 4.89% for spring. In the case of RF, overall disagreements ranged from 8.53% (summer) to 12.72% (autumn).

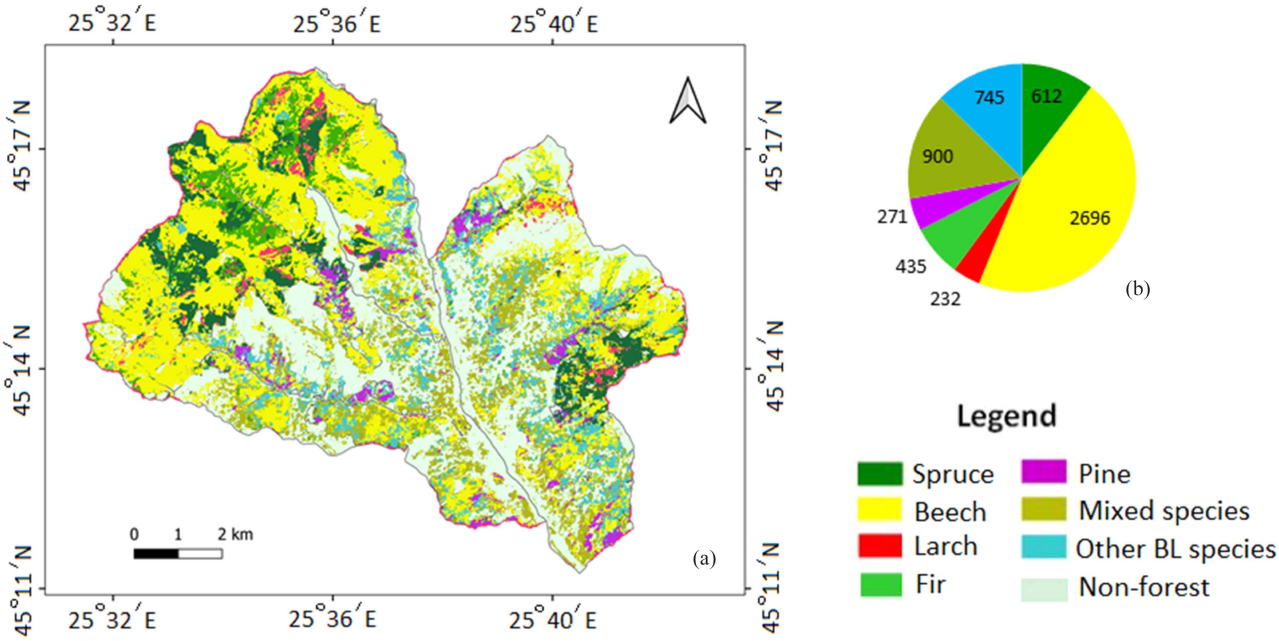

Fig. 5. (a) Map depicting the distribution of tree species for long-term interval in scenario 4, where the GTB algorithm ensured the best accuracies. (b) Pie chart represents the areas (in hectares) occupied by tree species.

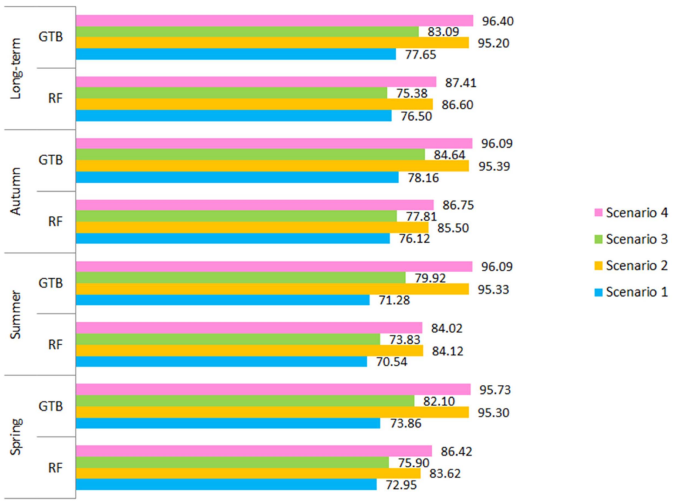

Fig. 6. OAs (%) obtained from applied ML algorithms in the four scenarios.

C. Tree Species Level Accuracy Assessment

The accuracy with which each tree species was identified by each algorithm varies considerably (see Fig. 11). Regardless of the analyzed scenario, time intervals, and ML algorithms, the highest values for UA and PA were obtained for beech (UA ranging from 70.28% to 95.38%; PA ranging from 90.38% to 98.91%), followed by spruce (UA ranging from 77.01 to 98.50; PA ranging from 79.52% to 98.62%). The lowest UA and PA values were obtained for the mixed species class (UA between 35.55% and 98.10% and PA between 7.57% and 90.00%), as well as for the other BL species class (UA between 46.42% and 98.95% and PA between 18.75% and 85.27%) (see Fig. 11). The highest F1 score values were obtained for spruce (98.40%), followed by beech (97.26%), while the lowest values were for mixed species (13.88%) and other BL species (29.93%) (see Fig. 9).

RF applied for all time intervals shows that the lowest values of UA, PA (see Fig. 11), and F1 score (see Fig. 9) were generally obtained for scenarios 1 and 3. Better results for UA, PA, and F1 score were obtained for scenarios 2 and 4. These results suggest that topographic data significantly contributed to distinguishing between tree species at different altitudes. Discrimination was observed for all tree species, but it was particularly pronounced for fir, pine, mixed species, and other BL species. For example, when applying the GBT algorithm, for scenario 4, the UA for other BL species increased by 29.08%pt. compared to scenario 3, while PA increased by 33.55%pt. (see Fig. 11).

The confusion matrices of the best classifications, namely for GTB and RF (scenario 4, long-time), are presented in Tables VII and VIII. In both GTB and RF cases, most confusions occurred between beech, mixed species, and other BL species. For example, in GTB, out of 57 pixels from the mixed species class, 48 were correctly classified, 4 as beech, 4 as other BL species, and 1 as pine. For RF, out of 52 pixels representing mixed species, 31 were correctly classified, 14 were assigned to the beech class, 5 to other BL species, and 1 each to spruce and pine classes. In the case of other BL species, confusions were higher; out of 95 reference pixels representing this class, 54 were correctly classified as other BL species and 33 as beech.

For each classification result, we calculated the importance of the variables. In Fig. 10, the importance of variables is presented by applying RF and GTB for scenario 4.

Fig. 7. Differences in OAs (%pt.) between (a) scenario 2 and scenario 1, (b) scenario 3 and scenario 1, (c) scenario 4 and scenario 1, (d) scenario 4 and scenario 2, and (e) scenario 4 and scenario 3.

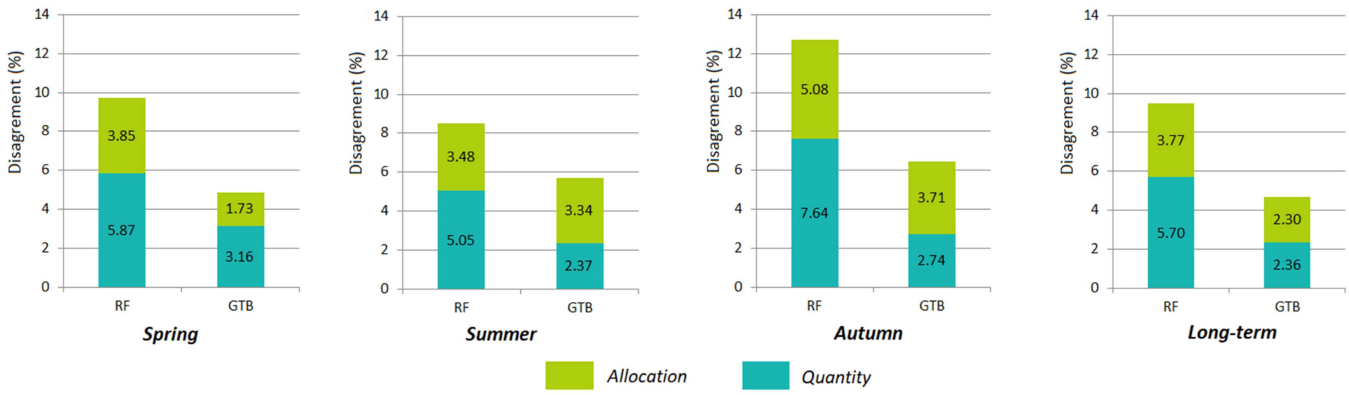

Fig. 8. Allocation and quantity disagreement components (in percentages) in scenario 4 for RF and GTB algorithms.

V. Discussion

A. Assessing Capabilities of ML Algorithms

Considering the analyzed scenarios and time-scale intervals, as well as the optimal parameters found, the highest accuracies were achieved with GTB followed by RF. Some differences were encountered between GBT and RF at the tree species level accuracy assessment (see Fig. 11).

GTB performed the best despite the current limitation of Ntree in GEE to less than 200. The high performance of GTB was attributed to its ability to model complex relationships between classes in satellite images, as well as to build complex models based on the large datasets used. In addition, GTB managed the variability and heterogeneity of data in S-2 images well, including variations in lighting conditions, atmospheric distortions, and noise. Georganos et al. [50] demonstrated that implementing XGboost in GTB, especially based on an extended set of features, systematically outperforms RF. However, there are studies in the literature showing that RF has outperformed GTB, but the increase in OA was only 0.14%pt. [3]. As demonstrated by the

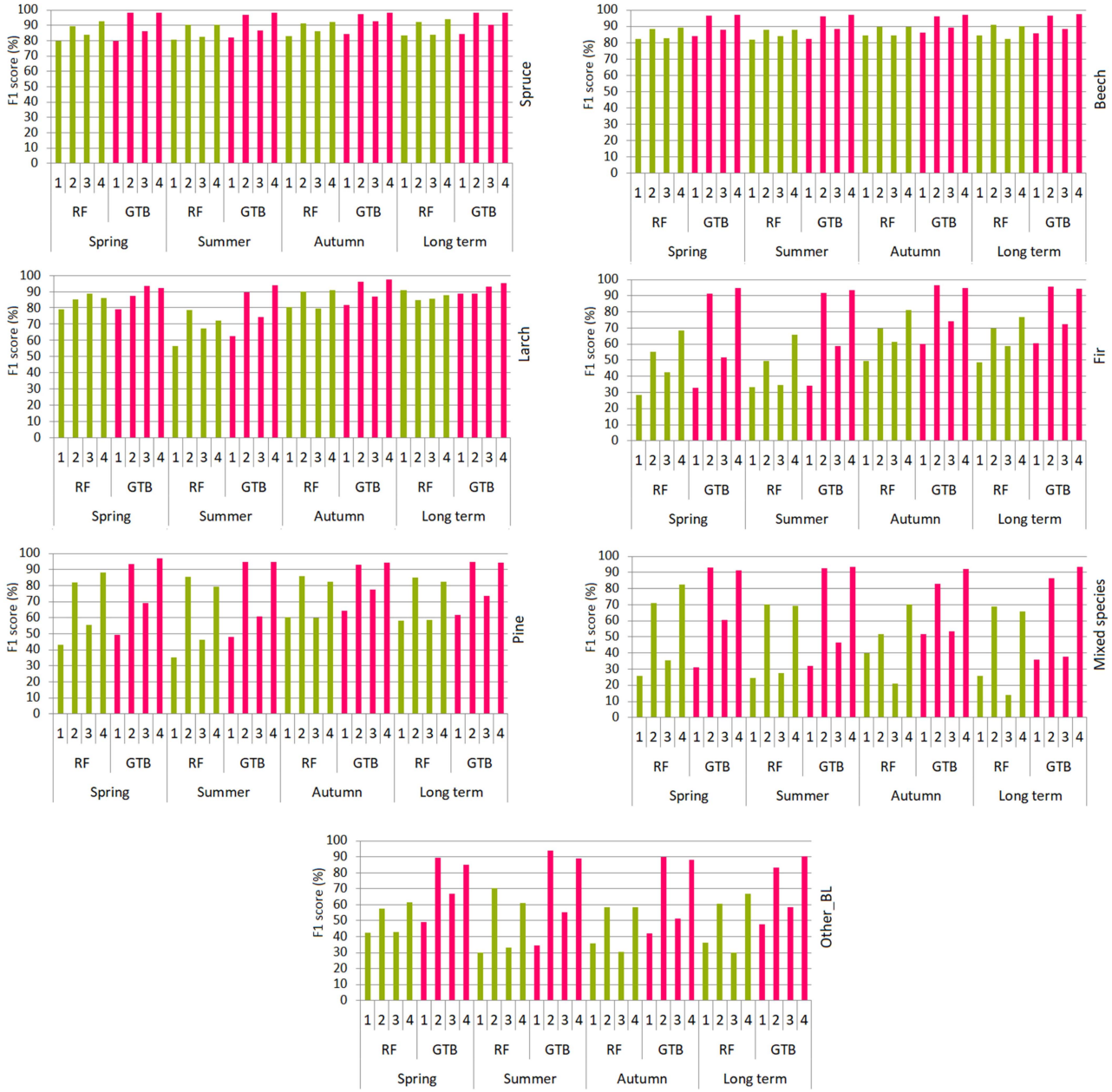

Fig. 9. F1 score obtained after applying ML algorithms for the seven tree species.

tuning results for GTB, the significance of parameter tuning also relies on the quality of the training dataset [45].

RF is a very popular algorithm, which is often faster compared to others, and does not require advanced hyperparameter tuning [44]. Regarding the RF parameter of Ntree in this study, the results showed that maximum OAs were achieved, for certain datasets, when Ntree was set in the range of 50–600. Obtaining lower OAs by RF compared to GTB may be due to the difficulties faced by the algorithm in the case of less common classes and imbalanced training data, as highlighted in other studies [23]. In addition, RF is not so robust to a small number of training samples, and it is possible that their number was smaller, insufficient for this algorithm.

The locations of each class in the classified maps were best identified by GTB, in the spring interval, which exhibited the lowest value for allocation disagreement (1.73%, representing 35.38% of the overall disagreement), followed by the long-term interval (2.30%, representing 49.36% of the overall disagreement). The quantity disagreement values were also low, ranging between 2.36% and 3.16%, indicating that the number of pixels in the classified map was close to that in the forest management map. Thus, through the optimal parameters set, the algorithm managed to separate the classes most effectively.

In the case of RF, the allocation disagreement values ranged from 3.48% to 5.08%, indicating that many areas were classified in locations where they were not observed. In this situation, the

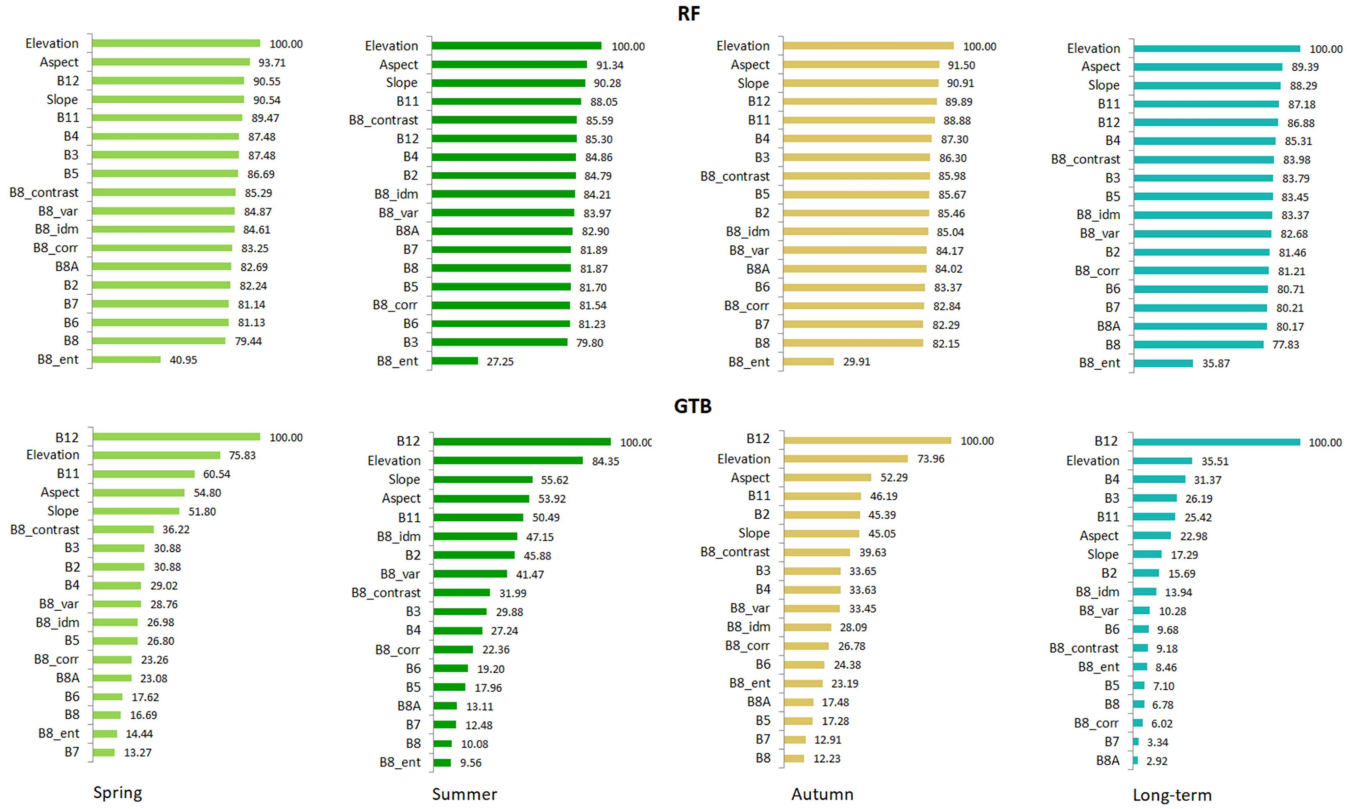

Fig. 10. Importance of variables used in classification applying ML algorithms for every analyzed time interval (scenario 4).

TABLE VII
CONFUSION MATRIX FOR GTB CLASSIFICATION IN SCENARIO 4 AND LONG-TIME INTERVAL

	Classification data								Total (number of pixels)	PA (%)
	Classes	Spruce	Beech	Larch	Fir	Pine	Mixed species	Other BL species		
Reference data	Spruce	**333**	1	1	0	3	0	0	338	98.52
	Beech	2	**609**	1	2	0	5	6	625	97.44
	Larch	1	2	**60**	1	0	0	0	64	93.75
	Fir	3	2	0	**102**	0	0	0	107	95.33
	Pine	2	0	0	0	**73**	0	0	75	97.33
	Mixed species	0	4	0	0	1	**48**	4	57	84.21
	Other BL species	0	6	0	1	1	0	**84**	92	91.30
Total (number of pixels)		341	624	62	106	78	53	94	**1309**	
UA (%)		97.65	97.60	96.77	96.22	93.59	90.57	89.36		
OA (%) = 96.40										

The bolded value along the main diagonal denotes the pixels accurately classified within each class.

most representative class is beech. It is possible that many areas classified by RF, which had mixtures of beech with different tree species, were allocated as beech. The discrepancies in quantity values for RF were consistently larger than those in allocation across all time intervals, indicating that the primary source of disagreement between the two maps was related to quantity errors rather than allocation errors at the pixel level. This indicates that the number of pixels predicted for each class differs substantially from the number of reference pixels. As a result, the RF algorithm delineates a larger area occupied by beech compared to the delineations produced by the GTB. Furthermore, the clear differences in the occupied areas are between beech, mixed species, and other BL species. This made the difference between algorithms, because in mixed species and other BL species, there is also beech that could not be separated and attributed to the beech class.

Fig. 11. UAs and PAs for the seven tree species identified in the study area.

TABLE VIII
CONFUSION MATRIX FOR RF CLASSIFICATION IN SCENARIO 4 AND LONG-TIME INTERVAL

	Classification data								Total (number of pixels)	PA (%)
	Classes	Spruce	Beech	Larch	Fir	Pine	Mixed species	Other BL species		
Reference data	Spruce	**313**	19	0	3	3	0	0	338	92.60
	Beech	0	**615**	1	2	2	2	3	625	98.40
	Larch	1	10	**45**	0	0	0	0	56	80.36
	Fir	20	32	0	**63**	0	0	0	115	54.78
	Pine	8	3	0	0	**66**	0	0	77	85.71
	Mixed species	1	14	0	0	1	**31**	5	52	59.61
	Other BL species	1	33	0	2	2	3	**54**	95	56.84
Total (number of pixels)		344	726	46	70	74	36	62	**1187**	
UA (%)		90.99	84.71	97.83	90.00	89.19	86.11	87.10		
OA (%) = 87.41										

The bolded value along the main diagonal denotes the pixels accurately classified within each class.

B. Assessing Different Scenarios

The different input variables led to different classification outcomes. Using only the S-2 bands (scenario 1) led to the highest OA achieved by the GTB algorithm (78.16%, autumn); the lowest OA was obtained by RF (70.54%, summer). The OAs obtained in scenario 1 were the lowest among all scenarios, except for one situation encountered in scenario 3 (RF, long-term), when they exceeded these (see Fig. 6). The use of rich spectral information obtained solely from the S-2 image bands plays an important role in tree species identification [51]. Compared to OA obtained using a single image, utilizing dense time-series S-2 images in tree species identification leads to higher OAs. In the study conducted by Persson et al. [8], using RF classifier and multitemporal S-2 images in identifying common tree species in Sweden, an OA of 88.2% was achieved. Grabska et al. [52] obtained an OA of 92.38% by combining five S-2 images taken in spring, summer, and autumn, and using all available images led to an OA of 92.12%.

Adding topographic data to the S-2 bands (scenario 2) resulted in a substantial increase in OAs, and consequently in better tree species identification. For example, using only S-2 multitemporal composites, in the case of GTB and the long-time interval, resulted in an OA of 77.65%, and adding the DEM layer improved the OA to 95.20% (see Fig. 6). The results obtained are in line with those in the literature. In the study conducted by Hościło and Lewandowska [13], it is shown that by combining topographic data with multitemporal S-2 images, for the classification of eight tree species, OA increased from 75.6% to 81.7%. Liu et al. [42] demonstrated that by combining multitemporal Landsat-8 and S-2 imagery with topographic data for the classification of four tree species and mixed forest types, an OA of 82.8% was achieved; OA increased by 15.2%pt. by adding topographic data compared to a single image. Dorren et al. [53] demonstrated that including topographic data in forest type classification can improve OA from 64% to 73%. In addition, other studies have shown the beneficial use of topographic data in increasing OA [3], [14], [54].

The texture information extracted from the multispectral S-2 images played a relatively minor role in tree species identification compared to topographic data. The contribution of texture features in combination with S-2 images (scenario 3) ranged between 1.69%pt. (RF, autumn) and 8.64%pt. (GTB, summer). Moreover, adding texture features led, in one case, to a decrease in OA by 1.12%pt. (RF, long-term) [see Fig. 7(b)]. The marginal contribution of texture features was also encountered in scenario 4, where OAs increased between 0.43%pt. (GTB, spring) and 2.80%pt. (RF, spring) compared to OAs in scenario 2 [see Fig. 7(d)]. In the summer interval, for RF, adding texture features led to a decrease in accuracy by 0.10%pt. The results obtained are similar to those in other studies. In the study conducted by You et al. [3], the addition of texture information improved the model accuracy by 3.10%pt. (for GTB) and by 1.89%pt. (for RF). Although, in the current study, GLCM textural features did not result in a significant increase in OAs, their contribution in scenario 4 was marginal; they contributed to the increase in UAs of mixed species and other BL species. In this regard, texture features have shown their capability of detecting the variability of forest species at the stand level.

Using S-2 spectral bands in combination with topographic data and texture features (scenario 4) led to the highest OAs (see Fig. 6), and consequently to a better identification of tree species. The variables used in the classification of tree species in this scenario had different contributions (see Fig. 10). Among the S-2 bands, the most important variables were B12, B11, B3, and B4, identified as crucial in other studies based on S-2 imagery related to tree species mapping [6], [8], [11], [12], [13], [15], [16], [17], [52]. Bands B11 and B12 were found to be sensitive to needle water content [55], canopy leaf water content [56], and lignin, starch, and nitrogen [20]. Since vegetation water content is closely related to phenology, this was reflected in the reflectance in the SWIR [57]. The visible red part of the spectrum is also sensitive to chlorophyll content. However, the red-edge bands, although related to vegetation leaf properties such as photosynthetic pigments, biomass, and structural carbohydrates [58], did not have a significant contribution to the current study.

Topographic data in scenario 4 had the highest contribution to tree species classification, with elevation ranking first, followed by aspect and slope (see Fig. 10). Adding topographic data as an auxiliary to satellite images can facilitate tree species identification, especially in mountainous areas with complex species composition, heterogeneous forest structures, and spatial variability in phenology [14], [18]. This is because the same tree species may exhibit different morphology and phenology in different growing seasons, depending on elevation, which results in their spectral characteristics differing locally [18].

The contribution of texture features in tree species identification was small. Among these, CON (B8_contrast), VAR (B8_var), and HO (B8_idm) showed the highest contribution to the classification accuracy among the GLCM texture, while COR (B8_corr) and EN (B8_ent) showed the lowest (see Fig. 10). The minimal contribution of EN suggests that the S-2 images were not complex, meaning they did not have a highly diverse distribution of gray values that would highlight their features. Therefore, texture information obtained for the study area from S-2 images with spatial resolutions of 10 and 20 m seems insufficient for such analyses. Adding texture features as variables in classification is more suitable for classifying details that are significantly larger than the spatial resolution of the remote sensing data. In the case of pixel-based analyses, texture features are less significant, especially if the pixel size is the same as or larger than the size of the recorded detail. Using satellite images with high spatial resolution provides richer texture information and allows for obtaining details related to size, canopy shape, and roughness, thereby enabling more precise identification of tree species [2]. This underscores the delicate balance between adding texture features as auxiliary layers of information for tree species identification and the noise introduced by their addition, which can affect classification accuracy [45]. However, in the study conducted by Nasiri et al. [4], it is shown that including forest stand textural and structural features can help highlight vertical and horizontal patterns among different species groups.

C. Comparison Between Time-Scale Intervals

The highest QAs, and thus a good separability between tree species, were obtained in the long-term interval (scenario 4, GTB), followed by those in autumn (scenario 4, GTB), with a difference of only 0.31%pt. between the two OAs. Moreover, the maximum difference in OAs between seasonal intervals for GTB was 0.67%pt., while for RF, it was 3.40%pt, both for scenario 4. The spring and summer combinations, regardless of the algorithm and scenario used, were not effective in distinguishing species in the analyzed area. These findings contrast with other studies that emphasized the superior accuracy of seasonal spectral-temporal metrics followed by monthly acquisitions [4], [14].

The reasons for the low performance of tree species identification in the seasonal intervals can likely be attributed to various factors. Large areas are characterized by highly diverse species composition, forest patterns, and management practices, as well as environmental conditions [14]. The timing of phenological events differs across the study region, especially if the altitudinal gradient is large. This is particularly relevant for spring and autumn composites when changes are more rapid. In addition, the phenology of tree species is controlled by factors such as photoperiod, winter chilling, altitude, and temperature [59]. In the studied area, the altitudinal distribution of tree species ranges from 530 to 1340 m a.s.l., resulting in phenological phases being shifted even for the same species. Although topographic data ensured that the sample plot belonged to the class based on the precise location and distribution range of tree species, confusions still occurred in classifications. This was encountered in beech and other species mixed with mixed species and other BL species, such as maple, birch, gray alder, black alder, and European hornbeam located across the entire area in various shares.

Another reason for the low accuracy in seasonal intervals for tree species identification could be the limited number of S-2 bands used to create the composites. This led to the data not being sufficiently precise or correctly synchronized with field processes. Although most S-2 images were captured in spring, when important phenological events such as leafing occur, the OAs of GTB (scenario 4) were the lowest (95.73%). Similarly, in summer, the OAs were also the lowest, indicating that phenology had little effect on species identification; moreover, there were fewer S-2 images available. Although phenological stages provided by seasonal scenarios can improve the spectral separability between tree species [4], the results of this study showed that combining phenological stages led to better separability.

Studies on tree species identification have yielded different results. Xi et al. [51] found that S-2 images captured in May, June, and July were more sensitive to phenological variations of tree species. Immitzer et al. [12] also concluded that images captured in April, May, and June were much more beneficial for tree species classification. Persson et al. [8] found that images from late spring and early summer were optimal for discriminating tree species. Grabska et al. [52] highlighted that the combination of spring and autumn led to good species discrimination. Hościło and Lewandowska [13] found that midautumn imagery was the best for tree species classification. Spectral variations in these months represented temporal dynamic differences in crown structure and biochemical characteristics among different tree species [13]. This is probably because phenological variations are much easier to capture using multitemporal imagery, such as S-2. Somewhat similar results to those of the present study were obtained by Grabska et al. [52] through the combination of S-2 images captured in spring and autumn (April 30/May 5/October 14/October 17/November 8). In addition, they showed that using a time series of S-2 images instead of single-date imagery significantly improved OA by approximately 5%–10%pt. in terms of tree species identification.

Therefore, although the best results were obtained in the long-time interval using the GTB algorithm, the differences in OA compared to the other time intervals were small, with a margin of only 0.67%pt. It is possible that certain specific phenophases of each season were captured in the long-term interval but were slightly shifted from each other. All these small discrepancies, considered for each season and combined, led to the best results in the long-term interval. However, some studies recommend

using dense time series to capture rapid phenological changes [14]. In addition, using satellite images from multiple years could help obtain compositions that facilitate better tree species identification. This underscores the complexity of identifying the optimal input variables in the temporal domain, which may explain why the long-term scenario outperforms the seasonal scenarios in this study.

D. Tree Species Identification

Identifying tree species using multitemporal S-2 images relies on capturing phenophases, such as budburst, leaf unfolding, autumn coloring, and abscission [60]. The spectral separability between different tree species increases at certain times related to phenological stages [8], and variations in the spectral behavior of tree species in different phenological stages are beneficial for their identification. For deciduous trees, the most important phenophase occurs during autumn and is related to leaf coloring. In addition, spring is characterized by another important phenophase, namely leaf emergence and greening. Although this study utilized most S-2 images acquired in spring (April and May) and autumn (October and November), and scenarios were analyzed for each season separately, considering phenophases individually did not aid in identifying tree species, except when considered together (long-time interval). It is possible that these phenophases either were not captured by the images used at their peak or that this point occurred between satellite passes. Thus, the timing of image acquisition outweighs the significance of image quantity [61]. Also, by using composites created by combining the bands of S-2 images taken during the analyzed time intervals, it is possible that not all phenological differences were captured.

The tree species that were best identified were spruce and beech, located in forests with homogeneous structures, of the same age, and having only one tree species in composition (see Fig. 11). These are compact stands generally found in the upper part of the study area. Considering the elevational gradient, although topographic data were used, differences still appeared even within the same species. These were caused by variations in reflectance determined by tree age, crown openness, local site conditions, stress, shadow effects, and crown health [52]. In addition, factors such as elevation, aspect, and soils influenced growth conditions, which in turn affected spectral variability within the same species [52]. Some studies have shown that broadleaf species, especially oak and birch, are elevation-dependent, while birch is sensitive to slope [13], [62], [63]. Furthermore, differences in the chemical and physical properties of tree species are reflected in the distinct spectral response, which constitutes the main driver for discriminating species [64].

Analyzing confusion matrices reveals that most confusions occurred between mixed species, other BL species classes, and beech (see Tables VII and VIII). Tree species in these classes, located at lower altitudes, are found in forests with heterogeneous structure, high fragmentation, and posed challenges in collecting accurate training samples. The presence of hornbeam, oak, birch, ash, and beech in intimate mixtures led to the collection of a mixed spectral signature. Moreover, spectral similarities among beech, hornbeam, alder, maple, oak, and ash contributed to inaccurate identification of mixed species and other BL species. This phenomenon is emphasized in other studies [52], [61], [65]. Furthermore, the training sample size for the mixed species class was smaller (see Table II). Some studies have demonstrated that small classes tend to be misclassified [52], [66], [67].

The phenophases in spring can be shifted even within the same species. For a species located at lower altitudes, leaf emergence and greening began earlier compared to the same species at higher altitudes, with temperature being the decisive factor [68], [69]. In the case of beech, located at lower altitudes, leafing depended on March temperatures, while for higher altitudes, it depended on April temperatures [68], [69]. In addition, some species such as hornbeam and beech are characterized by very similar phenological phases [68], [69], making phenological differences difficult to detect, as noted in other studies [70]. All these interspecific similarities led to lower accuracies for these classes. Moreover, the resolution of S-2 images does not allow the identification of such small groups of tree species [52].

For other BL species, located in the lower part of the study area, the forest is fragmented, has a more complex structure, and alternates with pastures, meadows, and built-up areas. These do not form large and homogeneous stands, and it is possible that marginal pixels from other land cover classes were included in the training samples, classified as forest in the nonforest map. Furthermore, the study by Wessel et al. [6] shows that using S-2 images allows for good results for forests with less complex structures and background signal effects.

Using topographical data in tree species identification requires the presence of reference data that cover the entire altitudinal range for each tree species or group of species from the lowest to the highest point of the current distribution of these species. In the present study, spruce, beech, fir, and mixed species are spread across the entire area, and for these, reference samples were distributed throughout their range. In contrast, for larch and pine, the reference samples were located only in a few locations where these two species are found. In addition, in the case of other BL species, which are located in the lower and central parts of the studied area, the reference samples were made in these parts. Under these conditions, for this tree species, it is possible that the models may be affected because using decision tree-based algorithms will be biased, as decision trees generally do not extrapolate.

E. Tree Species Identification in Forest Management

In forest management planning, tree species identification is essential. This constitutes the primary objective in forest inventory, alongside the collection of dendrometric data. Within the forest management plan, stand maps depict tree species and the composition of each forest unit, but obtaining maps using satellite imagery allows for their precise localization within the forest unit. Thus, by understanding the composition and distribution of tree species, a comprehensive and systematic perspective on forests is provided, enabling the monitoring and assessment of changes over time.

Implementing silvicultural management activities, including treatments, constitutes crucial actions for the future of forests. Planning and monitoring these activities using S-2 images as cartographic support can offer a significant advantage. For example, in the studied area of FMU I Comarnic, 1564.5 ha of forests [68] are included in the forest management plan where silvicultural treatments can be applied. Understanding species distribution, including within mixed stands, is important in determining cutting regimes to ensure natural regeneration, maintain an optimal mix of tree species, and eliminate invasive species. Simultaneously, this can help in planning sustainable management practices for mature forests that take into account the needs of different species to maintain a high level of biodiversity. By understanding changes in tree species distribution, decision-makers in forestry can adopt various strategies for forests to adapt to climate change.

The ecosystem services provided by forests in the studied area are undeniable and must be considered in forest management. One of these services is conservation, given that the forests are adjacent to or part of the protected area of the Bucegi Natural Park. From the forests within FMU I Comarnic, 19.7% (411.4 ha) are subject to conservation efforts, whereas within FMU II Posada, 98.5% (837.9 ha) are dedicated to conservation [68], [69]. Furthermore, 442.1 ha of FMU II Posada [69] are included in the Natura 2000 site ROSCI0013 Bucegi. In addition, 285.9 ha of forest [69] serve as buffer zones for reserves in the Bucegi Natural Park. Apart from these, there are 94.7 ha [69] designated as seed production and forest gene pool conservation reserves. Habitats encountered in the studied area include southeastern Carpathian forests of spruce, beech, and fir with *Pulmonaria rubra*, and southeastern Carpathian beech forests with *Symphytum cordatum*, requiring conservation activities. By understanding tree species, specific conservation strategies can be developed by conservation specialists to protect and restore habitats, with particular emphasis on threatened or endemic species.

Soil and steep slope protection constitute another ecosystem service that requires tree species identification for forest management. In FMU II Posada, 162.1 ha [69] are located on slopes with gradients exceeding 30°, with some stands situated on rocks and scree slopes. Another 192.1 ha [69] are found on slopes with gradients up to 30°, situated on lithologically very vulnerable substrates to erosion and landslides. In this situation, it is important to know the original species composition for reintroducing the right tree species and promoting ecosystem resilience [71]. Strategies for planting and regenerating forests in accordance with species requirements are necessary to prevent negative effects, such as insect attacks or fungal infections, which may occur when planting tree species outside their natural range.

Another ecosystem service offered by the studied forests is related to urban forests. In the lower and middle parts of the studied area, 257.9 ha [69] are included in the forest management plan and serve recreational and social interests. Considering the increasing expansion of urban areas and their status as tourist destinations, it is vital to maintain the role of these forests in ensuring air quality and quality of life in urban areas. Differences in the capacity of tree species to capture carbon dioxide from the atmosphere require their identification and inclusion in forest management. In this regard, forests play a crucial role in mitigating climate change by capturing and storing significant amounts of carbon [60], [72].

VI. Conclusion

In the present study, various scenarios of multitemporal S-2 imagery, ML algorithms, topographic data, and texture features were evaluated for tree species identification. The algorithms used were GTB and RF, both available on the GEE cloud computing platform. The results highlighted differences in the outputs of tree species identification due to classifiers, datasets, and time-scale intervals. The most accurate results were obtained by the GTB algorithm (over 95.70%) for all input datasets and time-scale intervals examined. Among these, the combination of S-2, topographic data, and textural features (scenario 4) for the long-term interval provided the best result (96.40%). The difference in OAs between the result obtained in the long-term interval and the weakest one obtained in spring, in the case of GTB, was only 0.67%pt. RF ranked after GTB, with a difference in OAs ranging from 8.31%pt. to 12.38%pt.

A significant increase in OA, and consequently in tree species identification, was achieved by introducing topographic data into the model. The contribution of texture features was marginal in increasing OAs but contributed to increasing UAs for mixed species and other BL species. Although images from different time-scale intervals were used, where phenological aspect is important, the best results were obtained in the long-time interval. To capture phenology, and thus ensure a more accurate identification of tree species, dense time series of S-2 images should be used.

The study relied on free S-2 images and the GEE platform, which enable the creation of a workflow that can be regularly used for mapping tree species. Such studies can be conducted at both local and regional levels. In this way, updated thematic maps can be prepared for forest management at various levels (forest unit, district unit). In addition, the studies can be used to promote sustainable forest management, monitor forest resource dynamics, and conserve biodiversity.

Acknowledgment

The author would like to thank Google Earth Engine for generously providing free services and the European Space Agency for providing Sentinel-2 images free of charge. The author would also like to thank the National Institute for Research and Development in Forestry Marin Drăcea, Romania, for providing the reference data. In addition, he would also like to thank the editor and reviewers for their invaluable contributions and dedication to this research.

References

[1] A. Axelsson, E. Lindberg, H. Reese, and H. Olsson, "Tree species classification using Sentinel-2 imagery and Bayesian inference," *Int. J. Appl. Earth Observ. Geoinf.*, vol. 100, 2021, Art. no. 102318, doi: 10.1016/j.jag.2021.102318.

[2] M. Ma, J. Liu, M. Liu, J. Zeng, and Y. Li, "Tree species classification based on Sentinel-2 imagery and random forest classifier in the eastern regions of the Qilian mountains," *Forests*, vol. 12, no. 12, 2021, Art. no. 1736, doi: 10.3390/f12121736.

[3] H. You, Y. Huang, Z. Qin, J. Chen, and Y. Liu, "Forest tree species classification based on Sentinel-2 images and auxiliary data," *Forests*, vol. 13, no. 9, 2022, Art. no. 1416, doi: 10.3390/f13091416.

[4] V. Nasiri, M. Beloiu, A. Asghar Darvishsefat, V. C. Griess, C. Maftei, and L. T. Waser, "Mapping tree species composition in a Caspian temperate mixed forest based on spectral-temporal metrics and machine learning," *Int. J. Appl. Earth Observ. Geoinf.*, vol. 116, 2023, Art. no. 103154, doi: 10.1016/j.jag.2022.103154.

[5] G. Kaplan, "Broad-leaved and coniferous forest classification in Google Earth Engine using sentinel imagery," *Environ. Sci. Proc.*, vol. 3, 2021, Art. no. 64, doi: 10.3390/iecf2020-07888.

[6] M. Wessel, M. Brandmeier, and D. Tiede, "Evaluation of different machine learning algorithms for scalable classification of tree types and tree species based on Sentinel-2 data," *Remote Sens*, vol. 10, no. 9, 2018, Art. no. 1419, doi: 10.3390/rs10091419.

[7] H. Costa, P. Benevides, F. D. Moreira, D. Moraes, and M. Caetano, "Spatially stratified and multi-stage approach for national land cover mapping based on Sentinel-2 data and expert knowledge," *Remote Sens.*, vol. 14, no. 8, 2022, Art. no. 1865, doi: 10.3390/rs14081865.

[8] M. Persson, E. Lindberg, and H. Reese, "Tree species classification with multi-temporal Sentinel-2 data," *Remote Sens.*, vol. 10, no. 11, pp. 1–17, 2018, doi: 10.3390/rs10111794.

[9] N. Puletti, F. Chianucci, and C. Castaldi, "Use of sentinel-2 for forest classification in Mediterranean environments," *Ann. Silvicultural Res.*, vol. 42, no. 1, pp. 32–38, 2018, doi: 10.12899/ASR-1463.

[10] G. Vaglio Laurin et al., "Species dominance and above ground biomass in the Białowieża Forest, Poland, described by airborne hyperspectral and Lidar data," *Int. J. Appl. Earth Observ. Geoinf.*, vol. 92, 2020, Art. no. 102178, doi: 10.1016/j.jag.2020.102178.

[11] M. Immitzer, F. Vuolo, and C. Atzberger, "First experience with Sentinel-2 data for crop and tree species classifications in central Europe," *Remote Sens.*, vol. 8, no. 3, 2016, Art. no. 166, doi: 10.3390/rs8030166.

[12] M. Immitzer, M. Neuwirth, S. Böck, H. Brenner, F. Vuolo, and C. Atzberger, "Optimal input features for tree species classification in central Europe based on multi-temporal Sentinel-2 data," *Remote Sens.*, vol. 11, no. 22, 2019, Art. no. 2599, doi: 10.3390/rs11222599.

[13] A. Hościło and A. Lewandowska, "Mapping forest type and tree species on a regional scale using multi-temporal Sentinel-2 data," *Remote Sens.*, vol. 11, no. 8, 2019, Art. no. 929, doi: 10.3390/rs11080929.

[14] E. Grabska, D. Frantz, and K. Ostapowicz, "Evaluation of machine learning algorithms for forest stand species mapping using Sentinel-2 imagery and environmental data in the Polish Carpathians," *Remote Sens. Environ.*, vol. 251, 2020, Art. no. 112103, doi: 10.1016/j.rse.2020.112103.

[15] A. Kollert, M. Bremer, M. Löw, and M. Rutzinger, "Exploring the potential of land surface phenology and seasonal cloud free composites of one year of Sentinel-2 imagery for tree species mapping in a mountainous region," *Int. J. Appl. Earth Observ. Geoinf.*, vol. 94, 2021, Art. no. 102208, doi: 10.1016/j.jag.2020.102208.

[16] P. Mohammadpour, D. X. Viegas, and C. Viegas, "Vegetation mapping with random forest using Sentinel 2 and GLCM texture feature—A case study for Lousã region, Portugal," *Remote Sens.*, vol. 14, no. 18, 2022, Art. no. 4585, doi: 10.3390/rs14184585.

[17] C. Bolyn, P. Lejeune, A. Michez, and N. Latte, "Mapping tree species proportions from satellite imagery using spectral–spatial deep learning," *Remote Sens. Environ.*, vol. 280, 2022, Art. no. 113205, doi: 10.1016/j.rse.2022.113205.

[18] X. Liu, J. Frey, C. Munteanu, N. Still, and B. Koch, "Mapping tree species diversity in temperate montane forests using Sentinel-1 and Sentinel-2 imagery and topography data," *Remote Sens. Environ.*, vol. 292, 2023, Art. no. 113576, doi: 10.1016/j.rse.2023.113576.

[19] J. Stoffels, S. Mader, J. Hill, W. Werner, and G. Ontrup, "Satellite-based stand-wise forest cover type mapping using a spatially adaptive classification approach," *Eur. J. Forest Res.*, vol. 131, pp. 1071–1089, 2012, doi: 10.1007/s10342-011-0577-2.

[20] F. E. Fassnacht et al., "Review of studies on tree species classification from remotely sensed data," *Remote Sens. Environ.*, vol. 186, pp. 64–87, 2016, doi: 10.1016/j.rse.2016.08.013.

[21] V. K. Rana and T. M. Venkata Suryanarayana, "Performance evaluation of MLE, RF and SVM classification algorithms for watershed scale land use/land cover mapping using Sentinel 2 bands," *Remote Sens. Appl. Soc. Environ.*, vol. 19, 2020, Art. no. 100351, doi: 10.1016/j.rsase.2020.100351.

[22] D. J. Lary, A. H. Alavi, A. H. Gandomi, and A. L. Walker, "Machine learning in geosciences and remote sensing," *Geosci. Front.*, vol. 7, no. 1, pp. 3–10, 2016, doi: 10.1016/j.gsf.2015.07.003.

[23] A. E. Maxwell, T. A. Warner, and F. Fang, "Implementation of machine-learning classification in remote sensing: An applied review," *Int. J. Remote Sens.*, vol. 39, no. 9, pp. 2784–2817, 2018, doi: 10.1080/01431161.2018.1433343.

[24] I. Vorovencii, "Long-term land cover changes assessment in the Jiului Valley mining basin in Romania," *Front. Environ. Sci.*, vol. 12, pp. 1–22, 2024, doi: 10.3389/fenvs.2024.1320009.

[25] R. M. Haralick, K. Shanmugam, and I. Dinstein, "Textural features for image classification," *IEEE Trans. Syst., Man, Cybern.*, vol. SMC-3, no. 6, pp. 610–621, Nov. 1973, doi: 10.1109/TSMC.1973.4309314.

[26] R. W. Conners, M. M. Trivedi, and C. A. Harlow, "Segmentation of a high-resolution urban scene using texture operators (Sunnyvale, California)," *Comput. Vis., Graph. Image Process.*, vol. 25, no. 3, pp. 273–310, 1984.

[27] F. Albregtsen, "Statistical texture measures computed from gray level coocurrence matrices," 2008. [Online]. Available: https://www.uio.no/studier/emner/matnat/ifi/INF4300/h08/undervisningsmateriale/glcm.pdf

[28] C. C. Gotlieb and H. E. Kreyszig, "Texture descriptors based on co-occurrence matrices," *Comput. Vis., Graph. Image Process.*, vol. 51, no. 1, pp. 70–86, 1990, doi: 10.1016/S0734-189X(05)80063-5.

[29] A. Humeau-Heurtier, "Texture feature extraction methods: A survey," *IEEE Access*, vol. 7, pp. 8975–9000, 2019, doi: 10.1109/ACCESS.2018.2890743.

[30] X. Zhang, J. Cui, W. Wang, and C. Lin, "A study for texture feature extraction of high-resolution satellite images based on a direction measure and gray level co-occurrence matrix fusion algorithm," *Sensors (Switzerland)*, vol. 17, no. 7, 2017, Art. no. 1474, doi: 10.3390/s17071474.

[31] M. Deur, M. Gašparović, and I. Balenović, "Tree species classification in mixed deciduous forests using very high spatial resolution satellite imagery and machine learning methods," *Remote Sens.*, vol. 12, no. 23, pp. 1–18, 2020, doi: 10.3390/rs12233926.

[32] C. I. Greșiță, "Expert system used for monitoring the behaviour of hydrotechnical constructions," *REVCAD J. Geod. Cadastre*, vol. 11, pp. 75–84, 2011.

[33] C. I. Greșiță, *Surveying Methods to Studying the Behaviour of Dams (in Romanian)*. Iasi, Romania: Tehnopress, 2013.

[34] C. C. Tereșneu, *Computer Aided Graphics (in Romanian)*. Brașov, Romania: Transilvania Univ. Press, 2019.

[35] G. M. Tudoran and M. Zotta, "Adapting the planning and management of Norway spruce forests in mountain areas of Romania to environmental conditions including climate change," *Sci. Total Environ.*, vol. 698, 2020, Art. no. 133761, doi: 10.1016/j.scitotenv.2019.133761.

[36] G. M. Tudoran, "Regulations regarding the management of forests included in natural protected areas," *Bull. Transilvania Univ. Brașov, II, Forestry Wood Ind. Agricultural Food Eng.*, vol. 55, no. 6, pp. 35–38, 2013.

[37] R. G. Pontius and M. Millones, "Death to Kappa: Birth of quantity disagreement and allocation disagreement for accuracy assessment," *Int. J. Remote Sens.*, vol. 32, no. 15, pp. 4407–4429, 2011, doi: 10.1080/01431161.2011.552923.

[38] L. Breiman, "Random forests," *Mach. Learn.*, vol. 45, pp. 5–32, 2001, doi: 10.1023/A:1010933404324.

[39] C. Pelletier, S. Valero, J. Inglada, N. Champion, and G. Dedieu, "Assessing the robustness of random forests to map land cover with high resolution satellite image time series over large areas," *Remote Sens. Environ.*, vol. 187, pp. 156–168, 2016, doi: 10.1016/j.rse.2016.10.010.

[40] M. Belgiu and O. Csillik, "Sentinel-2 cropland mapping using pixel-based and object-based time-weighted dynamic time warping analysis," *Remote Sens. Environ.*, vol. 204, pp. 509–523, 2018, doi: 10.1016/j.rse.2017.10.005.

[41] M. Immitzer, C. Atzberger, and T. Koukal, "Tree species classification with random forest using very high spatial resolution 8-band worldview-2 satellite data," *Remote Sens.*, vol. 4, no. 9, pp. 2661–2693, 2012, doi: 10.3390/rs4092661.

[42] Y. Liu, W. Gong, X. Hu, and J. Gong, "Forest type identification with random forest using Sentinel-1A, Sentinel-2A, multi-temporal Landsat-8 and DEM data," *Remote Sens.*, vol. 10, no. 6, pp. 1–25, 2018, doi: 10.3390/rs10060946.

[43] V. Nasiri et al., "The influence of data density and integration on forest canopy cover mapping using Sentinel-1 and Sentinel-2 time series in Mediterranean Oak forests," *ISPRS Int. J. Geo-Inf.*, vol. 11, no. 8, 2022, Art. no. 423, doi: 10.3390/ijgi11080423.

[44] M. Belgiu and L. Drăgu, "Random forest in remote sensing: A review of applications and future directions," *ISPRS J. Photogrammetry Remote Sens.*, vol. 114, pp. 24–31, 2016, doi: 10.1016/j.isprsjprs.2016.01.011.
[45] C. A. Orieschnig, G. Belaud, J. P. Venot, S. Massuel, and A. Ogilvie, "Input imagery, classifiers, and cloud computing: Insights from multi-temporal LULC mapping in the Cambodian Mekong delta," *Eur. J. Remote Sens.*, vol. 54, no. 1, pp. 398–416, 2021, doi: 10.1080/22797254.2021.1948356.
[46] Q. V. Vu, V. H. Truong, and H. T. Thai, "Machine learning-based prediction of CFST columns using gradient tree boosting algorithm," *Composite Struct.*, vol. 259, 2021, Art. no. 113505, doi: 10.1016/j.compstruct.2020.113505.
[47] T. Chen and C. Guestrin, "XGBoost: A scalable tree boosting system," in *Proc. 22nd ACM SIGKDD Int. Conf. Knowl. Discov. Data Mining*, 2016, vol. 13/17, pp. 785–794, doi: 10.1145/2939672.2939785.
[48] J. Elith, J. R. Leathwick, and T. Hastie, "A working guide to boosted regression trees," *J. Animal Ecol.*, vol. 77, no. 4, pp. 802–813, 2008, doi: 10.1111/j.1365-2656.2008.01390.x.
[49] S. S. Heydari and G. Mountrakis, "Effect of classifier selection, reference sample size, reference class distribution and scene heterogeneity in per-pixel classification accuracy using 26 Landsat sites," *Remote Sens. Environ.*, vol. 204, pp. 648–658, 2018, doi: 10.1016/j.rse.2017.09.035.
[50] S. Georganos, T. Grippa, S. Vanhuysse, M. Lennert, M. Shimoni, and E. Wolff, "Very high resolution object-based land use-land cover urban classification using extreme gradient boosting," *IEEE Geosci. Remote Sens. Lett.*, vol. 15, no. 4, pp. 607–611, Apr. 2018, doi: 10.1109/LGRS.2018.2803259.
[51] Y. Xi, C. Ren, Q. Tian, Y. Ren, X. Dong, and Z. Zhang, "Exploitation of time series Sentinel-2 data and different machine learning algorithms for detailed tree species classification," *IEEE J. Sel. Topics Appl. Earth Observ. Remote Sens.*, vol. 14, pp. 7589–7603, 2021, doi: 10.1109/JSTARS.2021.3098817.
[52] E. Grabska, P. Hostert, D. Pflugmacher, and K. Ostapowicz, "Forest stand species mapping using the Sentinel-2 time series," *Remote Sens*, vol. 11, no. 10, pp. 1–24, 2019, doi: 10.3390/rs11101197.
[53] L. K. A. Dorren, B. Maier, and A. C. Seijmonsbergen, "Improved landsat-based forest mapping in steep mountainous terrain using object-based classification," *Forest Ecol. Manage.*, vol. 183, pp. 31–46, 2003, doi: 10.1016/S0378-1127(03)00113-0.
[54] S. H. Chiang and M. Valdez, "Tree species classification by integrating satellite imagery and topographic variables using maximum entropy method in a Mongolian forest," *Forests*, vol. 10, no. 11, 2019, Art. no. 961, doi: 10.3390/f10110961.
[55] C. Senf, D. Pflugmacher, P. Hostert, and R. Seidl, "Using Landsat time series for characterizing forest disturbance dynamics in the coupled human and natural systems of Central Europe," *ISPRS J. Photogrammetry Remote Sens.*, vol. 130, pp. 453–463, 2017, doi: 10.1016/j.isprsjprs.2017.07.004.
[56] C. J. Tucker, "Remote sensing of leaf water content in the near infrared," *Remote Sens. Environ.*, vol. 10, no. 1, pp. 23–32, 1980, doi: 10.1016/0034-4257(80)90096-6.
[57] J. L. Olsen et al., "Relation between seasonally detrended shortwave infrared reflectance data and land surface moisture in semi-arid Sahel," *Remote Sens.*, vol. 5, no. 6, pp. 2898–2927, 2013, doi: 10.3390/rs5062898.
[58] M. Mngadi, J. Odindi, K. Peerbhay, and O. Mutanga, "Examining the effectiveness of Sentinel-1 and 2 imagery for commercial forest species mapping," *Geocarto Int.*, vol. 36, no. 1, pp. 1–12, 2021, doi: 10.1080/10106049.2019.1585483.
[59] J. Tang et al., "Emerging opportunities and challenges in phenology: A review," *Ecosphere*, vol. 7, no. 8, pp. 1–17, 2016, doi: 10.1002/ecs2.1436.
[60] I. Vorovencii et al., "Local-scale mapping of tree species in a lower mountain area using Sentinel-1 and -2 multitemporal images, vegetation indices, and topographic information," *Front. Forests Glob. Change*, vol. 6, pp. 1–18, 2023, doi: 10.3389/ffgc.2023.1220253.
[61] R. A. Hill, A. K. Wilson, M. George, and S. A. Hinsley, "Mapping tree species in temperate deciduous woodland using time-series multi-spectral data.," *Appl. Vegetation Sci.*, vol. 13, no. 1, pp. 86–99, 2010, doi: 10.1111/j.1654-109X.2009.01053.x.
[62] A. Abdollahnejad, D. Panagiotidis, S. S. Joybari, and P. Surovỳ, "Prediction of dominant forest tree species using Quickbird and environmental data," *Forests*, vol. 8, no. 2, 2017, Art. no. 42, doi: 10.3390/f8020042.
[63] P. Liu et al., "Evaluating the potential of Sentinel-2 time series imagery and machine learning for tree species classification in a mountainous forest," *Remote Sens.*, vol. 16, no. 2, 2024, Art. no. 293, doi: 10.3390/rs16020293.
[64] Y. Xi, W. Zhang, M. Brandt, Q. Tian, and R. Fensholt, "Mapping tree species diversity of temperate forests using multi-temporal Sentinel-1 and -2 imagery," *Sci. Remote Sens.*, vol. 8, 2023, Art. no. 100094, doi: 10.1016/j.srs.2023.100094.
[65] V. J. Pasquarella, C. E. Holden, and C. E. Woodcock, "Improved mapping of forest type using spectral-temporal Landsat features," *Remote Sens. Environ.*, vol. 210, pp. 193–207, 2018, doi: 10.1016/j.rse.2018.02.064.
[66] D. Sheeren et al., "Tree species classification in temperate forests using Formosat-2 satellite image time series," *Remote Sens.*, vol. 8, no. 9, pp. 1–29, 2016, doi: 10.3390/rs8090734.
[67] Y. Sun, A. K. C. Wong, and M. S. Kamel, "Classification of imbalanced data: A review," *Int. J. Pattern Recognit. Artif. Intell.*, vol. 23, pp. 687–719, 2009, doi: 10.1142/S0218001409007326.
[68] "Forest Research and Management Institute," *Forest Management Plan of Forest Management Unit I Comarnic (in Romanian)*. Braşov, Romania: ICAS, 2013.
[69] "Forest Research and Management Institute," *Forest Management Plan of Forest Management Unit II Posada (in Romanian)*. Brasov, Romania: ICAS, 2013.
[70] B. Schieber, R. Janík, and Z. Snopková, "Phenology of four broad-leaved forest trees in a submountain beech forest," *J. Forest Sci.*, vol. 55, no. 1, pp. 15–22, 2009, doi: 10.17221/51/2008-jfs.
[71] I. V. Abrudan, *Afforestation (in Romanian)*. Braşov, Romania: Transilvania Univ., 2006.
[72] S. J. Goetz et al., "Mapping and monitoring carbon stocks with satellite observations: A comparison of methods," *Carbon Balance Manage*, vol. 4, pp. 1–7, 2009, doi: 10.1186/1750-0680-4-2.

Iosif Vorovencii received the Ph.D. degree in forestry from the Transilvania University of Braşov, Braşov, Romania, in 2005.

He is currently a Professor of remote sensing and photogrammetry with the Transilvania University of Braşov.

He is a regular reviewer for multiple journals, such as *Remote Sensing*, *European Journal of Remote Sensing*, *International Journal of Remote Sensing*, and so on. His research interests include land cover/land use changes, machine learning algorithm, and environment remote sensing.